THE JOURNAL OF PHYSICAL CHEMISTRY C
A JOURNAL OF THE AMERICAN CHEMICAL SOCIETY

pubs.acs.org/JPCC

Article

# Analysis of the Limits of the Optical Response of a Metallic Nanoparticle with Gain

Luis Cerdán and Alejandro Manjavacas*

Cite This: J. Phys. Chem. C 2023, 127, 2371−2378

Read Online

ACCESS | Metrics & More | Article Recommendations | Supporting Information

**ABSTRACT:** Metallic nanostructures endowed with optical gain are promising building blocks for the development of active nanophotonic devices with enhanced optical responses as well as for exploring novel phenomena such as parity-time symmetry and nonreciprocity. However, despite their potential, the complexity of these systems frequently demands the use of simplified gain models, whose range of applicability is not always clear. Here, tracing our steps toward the basics, we analyze the optical response of a small active metallic nanoparticle using an intuitive, yet accurate, semianalytical model that takes into account the inherent nonlinear nature of the gain. We evaluate the near- and far-field responses of the active nanoparticle as a function of both the pump and the probe field strengths. We show that, under weak probe fields, the optical response of the active nanoparticle is greatly enhanced with increasing pump strength. In contrast, when the probe field is strong enough to deplete the excited-state population of the gain medium, the nanoparticle becomes passive, irrespective of the pump strength. Our results help to delineate the limits of applicability of the linear models used to describe the effect of gain in plasmonic nanostructures, thus paving the way to exploit these systems for the development of new applications.

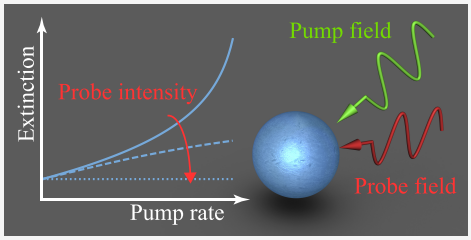


## INTRODUCTION

Thanks to their ability to support localized surface plasmons, nanostructures with free electrons have emerged as exceptional platforms to control light at the nanoscale. These excitations couple strongly to light and confine it in subwavelength volumes,[1] thus making the nanostructure that supports them display very large extinction cross-sections[2] and produce unparalleled near-field enhancements.[3] Therefore, metallic nanostructures are being used for a variety of applications: for example, to improve photocatalysis[4] and solar energy harvesting,[5] as well as to develop ultrasensitive optical sensors[6] and novel cancer therapies.[7] Nevertheless, the exceptional optical response provided by localized plasmons comes at the expense of relatively high levels of nonradiative losses arising from the metallic nature of the nanostructures that support them.[8]

The most natural solution to mitigate these losses consists in combining the plasmonic nanostructures with elements capable of providing optical gain.[9−12] These include, among others, semiconductor nanocrystals, dye molecules, and rare-earth ions, which, when externally pumped, can provide gain to the system.[13−19] Importantly, in addition to reducing the nonradiative losses, and therefore enhancing the response of the metallic nanostructure,[20−22] the incorporation of optical gain has enabled important applications such as the development of nanoscale light sources,[23,24] including a wide range of plasmonic nanolasers,[25−28] among which the spaser played a central role.[29−33] Furthermore, the modulation of the level of gain provides a mechanism to control the optical response of the plasmonic nanostructure, thus opening the door to the development of active nanophotonic devices.[34]

More recently, metallic nanostructures with gain are being combined with conventional, i.e., passive, metallic nanostructures, to build systems with parity-time symmetry.[35−37] The balance between active and passive responses in these systems results in extraordinary properties such as anisotropic emission[38−41] and scattering.[42−50] Unfortunately, in many cases, the complexity of the problem under investigation demands the use of simplified approaches to model the gain. These approaches usually describe the effect of gain through the inclusion of a term in the dielectric function with a negative imaginary part. While such level of description captures many of the key features introduced by the gain in the response of the metallic nanoparticle, it omits some important aspects. In particular, it is not able to describe in a self-consistent way the nonlinearity associated with the saturation of the gain, which plays a key role in the response of these systems[51−55] and can be exploited, for instance, to achieve nonreciprocal optical responses.[56] Although fully numerical approaches can be used to accurately describe these effects,[57,58] they are usually computationally demanding and many times do not offer an

Received: October 27, 2022
Revised: December 24, 2022
Published: January 25, 2023





https://doi.org/10.1021/acs.jpcc.2c07558
J. Phys. Chem. C 2023, 127, 2371−2378

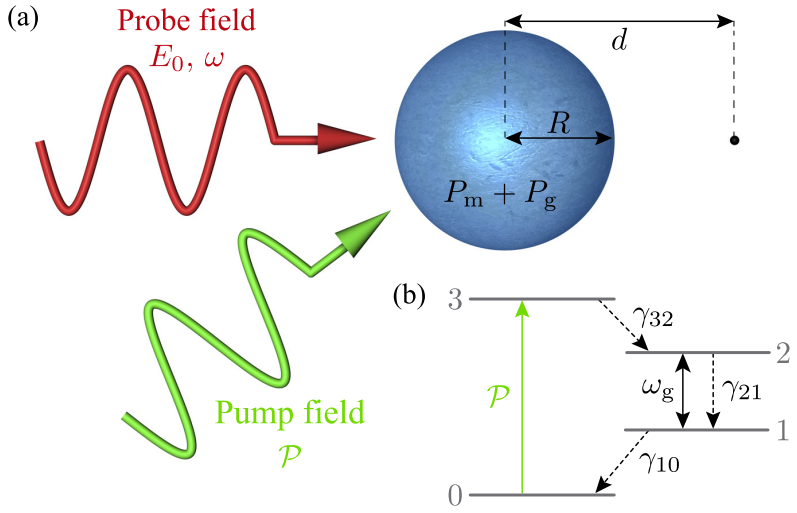


**Figure 1.** (a) Schematics of the system under consideration, consisting of a metallic nanoparticle doped with a gain medium. The nanoparticle is excited by a probe and a pump field. The black point at the right of the particle indicates the location where the field enhancement is calculated. (b) Energy level diagram for the gain medium.

appropriate level of insight into the relevant physical mechanisms.

Motivated by this, here, we use an intuitive but accurate semianalytical approach to perform a comprehensive analysis of the optical response of a small metallic nanostructure with gain. Our model is based on the combination of the semiclassical laser equations for the population dynamics of a 4-level system[59,60] with the electrostatic solution of the electromagnetic field of a nanosphere.[61] Using this model, which captures the intrinsic nonlinearity of the optical gain, we investigate the far- and near-field response of the active nanostructure as a function of the strength of the pump and the probe fields. We find that, for weak probe fields, the presence of gain results in a great enhancement of the optical response of the nanoparticle, which grows with the strength of the pump. On the contrary, under sufficiently strong probe fields, the excited-state population of the gain medium gets significantly depleted, thus making the nanoparticle become increasingly passive, regardless of the strength of the pump. Our results shed light on the plasmonic response of metallic nanostructures with gain and illustrate the limits to the enhancement of their response that can be achieved by the presence of gain. Therefore, our work facilitates the use of these active plasmonic nanostructures for the development of new applications, including enhanced optical sensing,[62−64] and the exploration of novel phenomena such as parity-time symmetry and nonreciprocity.

## METHODS

The system under study is depicted in Figure 1a. It consists of a spherical nanoparticle placed in vacuum, with a radius $R$ that is much smaller than any of the wavelengths relevant to our problem. The nanoparticle has a plasmonic nature arising from the presence of free electrons and an active character resulting from being doped with a gain medium. As we show later, these assumptions allow us to obtain an analytical solution of Maxwell's equations. We consider the nanoparticle to be incoherently excited by a pump field with rate $\mathcal{P}$ (green wavy arrow) and analyze its near- and far-field optical responses with a probe field of amplitude $E_0$ and frequency $\omega$ (red wavy arrow). Although the system might seem exotic, there are currently several potential approaches to develop plasmonic nanoparticles with gain employing known materials, such as co-doping of transparent conducting oxides[65] and semiconductor nanocrystals,[66] as well as exploiting the intrinsic luminescence of noble metals.[67−69] Nonetheless, the results that we present in the following are sufficiently general to be qualitatively extrapolated to more complex, but readily available, systems such as core−shell nanoparticles.

Unlike many other formalisms based on frequency-domain methods, here, we resort to a conventional time-domain approach to capture the nonlinear nature of the gain and then look for the steady-state solutions. We can distinguish two different contributions to the total polarization of the active plasmonic nanoparticle: one corresponding to the free electrons $\mathbf{P}_m$ and another from the gain medium $\mathbf{P}_g$. The dynamics of the former is described by

$$\frac{\partial^2 \mathbf{P}_m}{\partial t^2} + 2\Gamma_m \frac{\partial \mathbf{P}_m}{\partial t} = \frac{\omega_m^2}{4\pi}\mathbf{E}_t \tag{1}$$

where $\hbar\omega_m = 1.8$ eV is the plasma energy, $\Gamma_m = 0.05\omega_m$ its associated damping, and $\mathbf{E}_t$ is the total field inside the nanoparticle. These are typical values for transparent conducting oxides[65] or semiconductor nanocrystals.[66] Indeed, similar values have been previously used in the context of active plasmonics.[70] To model the gain medium, we use a conventional 4-level system, sketched in Figure 1b, with a single radiative transition $2 \rightarrow 1$ of frequency $\omega_g$ and linewidth $2\Gamma_g$. The medium is radiatively pumped through the transition $0 \rightarrow 3$ at a rate $\mathcal{P}$. Working with a pump rate instead of a pump field allows us to be agnostic to the pump intensity and frequency as well as the absorption properties of the gain medium. This approximation is justified in homogeneously broadened 4-level systems, in which the frequency of the pump field is sufficiently far from $\omega_g$.[59,60] The evolution of the polarization of the gain medium is given by

$$\frac{\partial^2 \mathbf{P}_g}{\partial t^2} + 2\Gamma_g \frac{\partial \mathbf{P}_g}{\partial t} + \omega_g^2 \mathbf{P}_g = -\sigma_g \Delta N \mathbf{E}_t \tag{2}$$



https://doi.org/10.1021/acs.jpcc.2c07558
J. Phys. Chem. C 2023, 127, 2371−2378

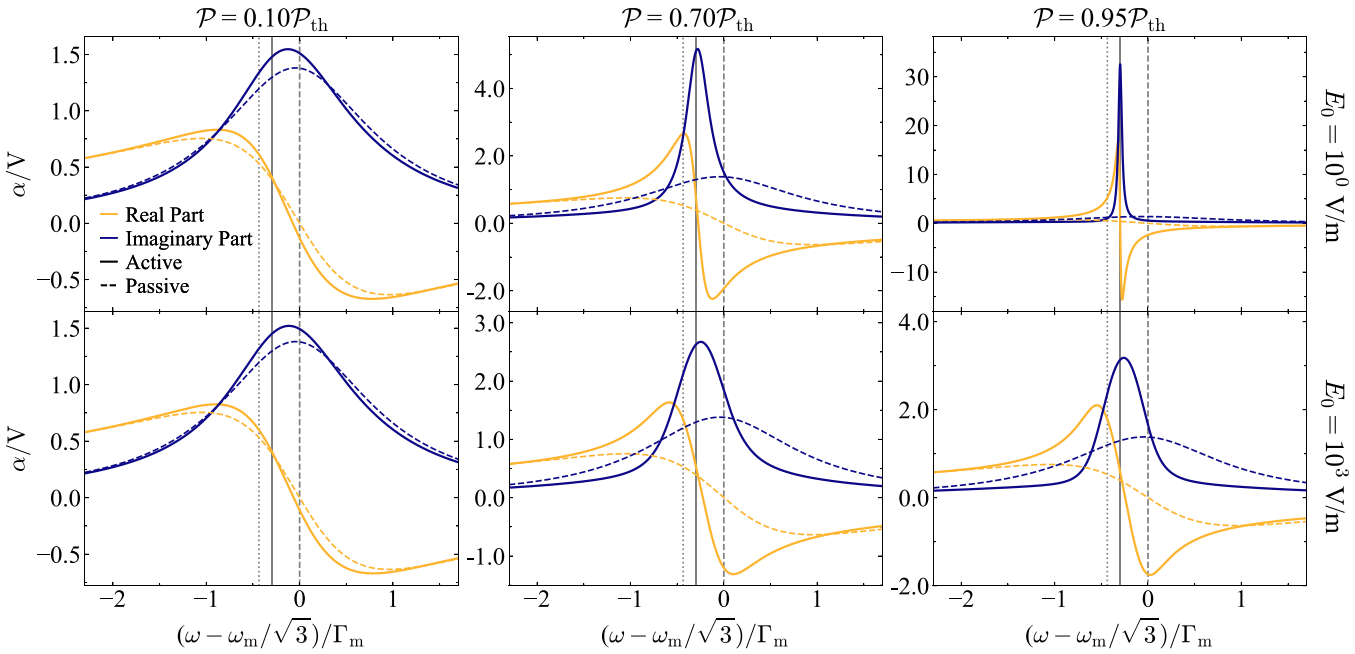


**Figure 2.** Polarizability of an active (solid curves) and a passive (dashed curves) plasmonic nanoparticle as a function of probe field frequency $\omega$ for the different values of the pump rate $\mathcal{P}$ (columns) and the probe field amplitude $E_0$ (rows) indicated in the labels. In all cases, we normalize the polarizability to the volume of the nanoparticle and use yellow and blue curves to denote respectively its real and imaginary parts. The dotted, solid, and dashed vertical lines mark the position of $\omega_g$, $\omega_l$, and $\omega_m/\sqrt{3}$, respectively (see text for details).

where $\Delta N = N_2 - N_1$ is the density of the population inversion between the levels involved in the radiative transition and $\sigma_g = 10^{10}$ cm$^3$ s$^{-2}$ is the field-matter coupling factor.[59] The dynamics of the population densities of the different levels $N_i$ ($i$ = 0, ..., 3) satisfies[60]

$$\begin{aligned}
\frac{dN_3}{dt} &= -\gamma_{32}N_3 + \mathcal{P}(N_0 - N_3)\\
\frac{dN_2}{dt} &= \gamma_{32}N_3 - \gamma_{21}N_2 + \frac{1}{\hbar\omega_g}\mathbf{E}_t\cdot\frac{d\mathbf{P}_g}{dt}\\
\frac{dN_1}{dt} &= \gamma_{21}N_2 - \gamma_{10}N_1 - \frac{1}{\hbar\omega_g}\mathbf{E}_t\cdot\frac{d\mathbf{P}_g}{dt}\\
\frac{dN_0}{dt} &= \gamma_{10}N_1 - \mathcal{P}(N_0 - N_3)
\end{aligned} \tag{3}$$

Notice that the sum of the population densities of all of the levels equals $N_t$, which is assumed to be constant. Furthermore, $\gamma_{ij}$ represents the decay rate of the transition $i \rightarrow j$, which includes both radiative and nonradiative contributions. The last term in the second and third rows of eq 3 accounts for the stimulated emission processes that arise from the interaction between the polarization of the gain medium $\mathbf{P}_g$ and the total electric field $\mathbf{E}_t$ inside the nanoparticle. Notice that, in the case of a radiative decay, our semiclassical model does not capture the contribution of the spontaneously emitted photon to the electric field. In our calculations, we assume $\hbar\omega_g$ = 1.0 eV, $\Gamma_g = 0.1\omega_g$, $\gamma_{21} = 10^9$ s$^{-1}$, $\gamma_{32} = \gamma_{10} = 10^{13}$ s$^{-1}$, and $N_t = 10^{19}$ cm$^{-3}$, which are compatible with gain media such as rare-earth ions and dye molecules.

The total field $\mathbf{E}_t$ that appears in eqs 1−3 corresponds to the sum of the probe field $\mathbf{E}_0$ and the field produced by the two components of the polarization $\mathbf{P}_m$ and $\mathbf{P}_g$. Since we assume that the size of the nanoparticle is much smaller than the relevant wavelengths, we can exploit the electrostatic approximation to solve Maxwell's equations. Within this limit and using Gaussian units, the total field inside the active nanoparticle is uniform and given by (see the Supporting Information)

$$\mathbf{E}_t = -\frac{4\pi}{3}(\mathbf{P}_m + \mathbf{P}_g) + \mathbf{E}_0 \tag{4}$$

Furthermore, given that the pump is assumed to be incoherent and the constituents of the gain medium are randomly oriented, all of the elements in the preceding equation are parallel to $\mathbf{E}_0$. This allows us to simplify the notation by considering the fields and polarizations as scalars and to decompose each of them as $F(t) = fe^{-i\omega t} + f^*e^{i\omega t}$, with $f$ being a slowly varying complex function, $f^*$ its complex conjugate, and $\omega$ the frequency of the probe field. Using this decomposition and substituting eq 4 into eqs 1−3, we arrive at a set of coupled second-order differential equations that can be readily solved to obtain the transient or time-dependent response of the active plasmonic nanoparticle (see the Supporting Information). Nevertheless, here, we are interested in finding the steady-state solution of the problem, with the twofold purpose of getting better insight into the behavior of the system and a direct comparison with the results of usual frequency-domain approaches. Under these conditions, and assuming $E_0$ to be constant and real, the steady-state (SS) solution of the two components of the polarization is

$$P_m^{SS} = \frac{\omega_m^2}{3}\frac{\frac{3}{4\pi}E_0 - P_g^{SS}}{\frac{\omega_m^2}{3} - \omega^2 - 2i\Gamma_m\omega} \tag{5}$$

$$P_g^{SS} = \frac{\sigma_g\Delta N^{SS}\left(\frac{4\pi}{3}P_m^{SS} - E_0\right)}{\omega_g^2 - \omega^2 - \frac{4\pi}{3}\sigma_g\Delta N^{SS} - 2i\Gamma_g\omega} \tag{6}$$



https://doi.org/10.1021/acs.jpcc.2c07558
J. Phys. Chem. C 2023, 127, 2371−2378

while the population inversion density is

$$\Delta N^{SS} = S\mathcal{P}\frac{N_t + \frac{2}{\gamma_{21}\hbar\omega_g}\mathrm{Re}\left\{ i\omega P_g^{SS}\left(E_0 - \frac{4\pi}{3}P_m^{SS}\right)^*\right\}}{\gamma_{10} + \mathcal{P}\left(2 + 2\frac{\gamma_{10}}{\gamma_{32}} + S\right)} - \frac{2}{\gamma_{21}\hbar\omega_g}\mathrm{Re}\left\{ i\omega P_g^{SS}\left(E_0 - \frac{4\pi}{3}P_m^{SS}\right)^*\right\} \quad (7)$$

with $S = (\gamma_{10} - \gamma_{21})/\gamma_{21}$. Notice that we have opted to garner all of the information regarding the population of the states within the steady-state population inversion density $\Delta N^{SS}$ because this quantity is what drives the polarization associated with the gain medium. Equations 5−7 effectively describe a single-mode plasmonic nanostructure with a homogeneously broadened gain. Furthermore, these equations form a system of coupled nonlinear equations that does not have a general analytical solution. However, it can be readily solved by converting it into a two-dimensional *root-finding* problem (see the Supporting Information).

## RESULTS AND DISCUSSION

The optical response of the active plasmonic nanoparticle upon excitation by the probe field is fully characterized by its polarizability $\alpha$. This quantity, which can be expressed as the ratio between the total dipole moment induced in the nanoparticle and the incident field, reads

$$\alpha = V\frac{P_m^{SS} + P_g^{SS}}{E_0} \quad (8)$$

where $V = 4\pi R^3/3$ is the volume of the nanoparticle. We begin our analysis by calculating the polarizability of a passive plasmonic nanoparticle, for which both $\mathcal{P} = 0$ and $P_g^{SS} = 0$. The corresponding results are shown in Figure 2 as a function of the probe field frequency $\omega$ and normalized to $V$. We use yellow and blue dashed curves to display respectively the real and imaginary parts of the polarizability. Notice that, because the polarizability of the passive plasmonic nanoparticle does not depend on the probe amplitude $E_0$, the dashed curves of all of the panels of Figure 2 are the same. Furthermore, for $\mathcal{P} = 0$ and $P_g^{SS} = 0$, eq 8 admits a simple analytical solution that coincides exactly with the usual expression for the polarizability of a small spherical nanoparticle, $\alpha = R^3(\varepsilon - 1)/(\varepsilon + 2)$ with $\varepsilon = 1 - \omega_m^2/(\omega^2 + 2i\omega\Gamma_m)$. Examining the dashed curves in Figure 2, we observe that, as expected, the polarizability of the passive plasmonic nanoparticle displays a resonance approximately located at $\omega_m/\sqrt{3}$, which corresponds to the localized plasmon of the nanoparticle.[1]

The incorporation of gain introduces important differences. To make our results as agnostic to the material parameters as possible, we characterize the level of gain through the pump rate $\mathcal{P}$, normalized to the laser threshold value $\mathcal{P}_{th}$. The latter denotes the pump rate for which the system transits into a lasing emission regime. The use of $\mathcal{P}$, normalized to $\mathcal{P}_{th}$, to characterize the level of gain not only allows us to perform meaningful comparisons between different systems but also prevents us from pumping the nanoparticle above its laser threshold, where the assumptions behind eqs 5−7 do not hold. This is in contrast to other simplified models, such as those based on the inclusion of a term in the dielectric function with a negative imaginary part, for which it is not always possible to accurately determine the laser threshold of the system. As a consequence, the level of gain is oftentimes increased beyond that threshold, even though doing so may break some of the approximations behind the model.[16] To calculate $\mathcal{P}_{th}$, as well as the laser frequency $\omega_l$, we perform a linear stability analysis of the differential equations governing the dynamics of the active plasmonic nanoparticle[71] in the absence of probe field $E_0$ (see the Supporting Information).

The solid curves in Figure 2 show the real (yellow curves) and imaginary (blue curves) parts of the polarizability of the active plasmonic nanoparticle for different values of the pump rate $\mathcal{P}$ (columns) and the probe field amplitude $E_0$ (rows). The panels in the top row display the results for a probe field $E_0 = 10^0$ V/m, which is not strong enough to deplete the excited-state population of the gain medium. Under these conditions, which are usually denoted as small-signal regime, the response of the nanoparticle is expected to be linear with respect to $E_0$ and to increase with the gain. For a small level of gain, $\mathcal{P} = 0.10\mathcal{P}_{th}$ (top left panel), the polarizability is very similar to the passive case, except for a small redshift of the plasmon frequency and a slight increase in its strength. In contrast, as the pump rate increases to $\mathcal{P} = 0.70\mathcal{P}_{th}$ (top middle panel) and then approaches the threshold value $\mathcal{P} = 0.95\mathcal{P}_{th}$ (top right panel), the linewidth of the plasmon resonance becomes increasingly narrow and its strength grows to reach a 20-fold increase with respect to the passive case. These results are in good agreement with previous theoretical and experimental observations in loss compensated systems and can be attributed to the effective reduction of the metallic nonradiative losses induced by the gain, which results in a much stronger plasmonic response. Furthermore, as $\mathcal{P}$ grows, the spectral position of the plasmon resonance converges toward the laser frequency $\omega_l$, where the amplification produced by the gain is more effective.

The response of the active plasmonic nanoparticle suffers important changes when the amplitude of the probe field is increased beyond the small-signal regime. The rise of $E_0$ produces an increase in the polarization of the free electrons and the gain medium. As a consequence, the population of level 2 gets depleted at a larger rate, thus reducing the value of $\Delta N^{SS}$ and, hence, the effect of the gain. This scenario is analyzed in the panels of the bottom row of Figure 2. There, we plot the polarizability of the active plasmonic nanoparticle for a probe field $E_0 = 10^3$ V/m. For the smallest value of $\mathcal{P}$ under consideration (bottom left panel), for which the effect of gain is not significant, the plasmon resonance barely changes with respect to the results for $E_0 = 10^0$ V/m (top left panel). However, as the pump rate grows, the differences between the results for $E_0 = 10^0$ V/m and $E_0 = 10^3$ V/m become increasingly large. In particular, while, for $E_0 = 10^0$ V/m, there is a huge enhancement of the polarizability when $\mathcal{P}$ approaches the threshold value (cf. top middle and top right panels), for $E_0 = 10^3$ V/m, the enhancement is very modest. Importantly, in this case, the polarizabilities for $\mathcal{P} = 0.70\mathcal{P}_{th}$ (bottom middle panel) and $\mathcal{P} = 0.95\mathcal{P}_{th}$ (bottom right panel) are very similar. This is the manifestation of a saturation effect, which has its origin in the nonlinear nature of the gain and the depletion effect that the probe field has on the population inversion of the gain medium. Even though the pump rate is increased from $0.70\mathcal{P}_{th}$ to $0.95\mathcal{P}_{th}$, the response of the nanoparticle does not improve significantly.



https://doi.org/10.1021/acs.jpcc.2c07558
J. Phys. Chem. C 2023, 127, 2371−2378

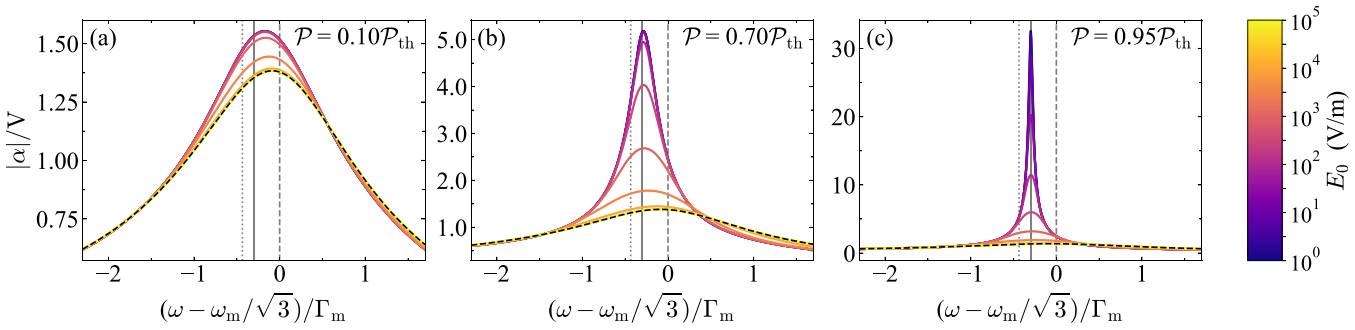


**Figure 3.** Absolute value of the polarizability of an active (solid colored curves) and a passive (dashed black curves) plasmonic nanoparticle as a function of the probe field frequency, $\omega$, for different values of the probe field amplitude, $E_0$ (see the color bar). We consider three different pump rates: $\mathcal{P} = 0.10\mathcal{P}_{th}$ (a), $\mathcal{P} = 0.70\mathcal{P}_{th}$ (b), and $\mathcal{P} = 0.95\mathcal{P}_{th}$ (c). The vertical lines follow the same notation as in Figure 2.

In order to gain more insight into the saturation effect caused by the increase of the probe field, we plot, in Figure 3, the absolute value of the polarizability for different probe field amplitudes $E_0$, ranging from $10^0$ to $10^5$ V/m. We consider the three different pump rates that we analyzed in Figure 2. Examining these results, we observe that, for all of the values of $\mathcal{P}$, the polarizability of the nanoparticle becomes broader and its value decreases globally as $E_0$ becomes larger. At the same time, the position of the peak converges toward $\omega_m/\sqrt{3}$. All of these trends are consistent with a gradual decrease in the effect of the gain, which becomes more pronounced the larger the value of $\mathcal{P}$ gets. For $E_0 \geq 10^4$ V/m, the polarizability becomes indistinguishable from that of the passive system, which is shown by the dashed black curves. Although the value of $E_0$ at which saturation happens depends on the particular choice of parameters, the trend described in Figure 3 is general. We can thus conclude that the increase in the level of gain results in larger enhancements of the response of the active plasmonic nanoparticle, but this comes at the price of suffering a stronger saturation effect that occurs at smaller values of the probe field amplitude.

Even though the polarizability contains all of the information to characterize the optical response of the active plasmonic nanoparticle, it is not a quantity that can be directly measured. To make our study more general, we extend our analysis to the near-field intensity enhancement and the extinction cross-section. These are two quantities that are usually employed to characterize respectively the near- and far-field response of a plasmonic nanostructure.[72] We define the near-field intensity enhancement $\eta$ as the ratio between the field intensity produced by the nanoparticle and the probe field intensity. We evaluate $\eta$ at a point located a distance $d$ from the center of the nanoparticle in the direction perpendicular to the polarization of the probe field, as indicated in the schematics of Figure 1a. Under these conditions, we have (see the Supporting Information)

$$\eta = \frac{V^2}{d^6}\frac{\left|P_m^{SS} + P_g^{SS}\right|^2}{|E_0|^2}$$

On the other hand, the extinction cross-section is given by[72]

$$\sigma_{ext} = 4\pi\frac{\omega}{c}V\ \mathrm{Im}\left\{\frac{P_m^{SS} + P_g^{SS}}{E_0}\right\}$$

Figure 4 shows $\eta$ and $\sigma_{ext}$ as a function of either the pump rate $\mathcal{P}$ or the probe field $E_0$. In the first case, we consider three

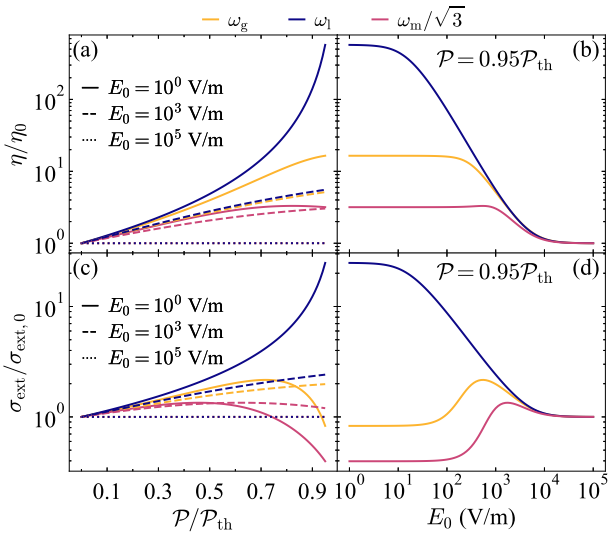


**Figure 4.** Near-field intensity enhancement $\eta$ (a, b) and extinction cross-section $\sigma_{ext}$ (c, d) of the active plasmonic nanoparticle plotted as a function of $\mathcal{P}$ (a, c) and $E_0$ (b, d). We normalize $\eta$ and $\sigma_{ext}$ to the values of the respective quantities for a passive nanoparticle $\eta_0$ and $\sigma_{ext,0}$. As indicated by the legend, the solid, dashed, and dotted curves in (a) and (c) correspond to $E_0 = 10^0$ V/m, $E_0 = 10^3$ V/m, and $E_0 = 10^5$ V/m, respectively, while in (b) and (d), we use $\mathcal{P} = 0.95\mathcal{P}_{th}$. In all of the panels, the yellow, blue, and red curves denote the results calculated respectively at $\omega_g$, $\omega_l$, and $\omega_m/\sqrt{3}$.

different values of $E_0$: $10^0$, $10^3$, and $10^5$ V/m, as indicated by the legends. In the second case, we set the pump rate at $\mathcal{P} = 0.95\mathcal{P}_{th}$. We perform the calculations at the three characteristic frequencies of the system $\omega_g$, $\omega_l$, and $\omega_m/\sqrt{3}$, as indicated by the top legend. To make the results more general, we normalize $\eta$ and $\sigma_{ext}$ to the corresponding results for the passive plasmonic nanoparticle, which we denote as $\eta_0$ and $\sigma_{ext,0}$, respectively.

Figure 4a,b displays the results for the near-field intensity enhancement $\eta$. It is well-known that the localized plasmons of metallic nanoparticles can produce large enhancements of the field in the vicinity of the nanostructure.[3] As expected, the addition of gain results in an increase of $\eta$. However, such an increase is largely dependent on the amplitude and frequency of the probe field. Following the results of Figures 2 and 3, the largest value of $\eta/\eta_0$ is expected to happen for the smallest $E_0$ and for frequencies close to $\omega_l$, where the effect of the gain is more effective. This is confirmed by the blue solid curve in Figure 4a, which shows that, for $E_0 = 10^0$ V/m and $\omega = \omega_l$, $\eta/$



https://doi.org/10.1021/acs.jpcc.2c07558
J. Phys. Chem. C 2023, 127, 2371−2378

$\eta_0$ reaches a value of ∼600 as the pump rate approaches $0.95\mathcal{P}_{th}$. At the other frequencies under consideration (yellow and red curves), the growth of $\eta$ with $\mathcal{P}$ is less pronounced. Similarly, the increase of $E_0$ to $10^3$ and $10^5$ V/m results in a drastic reduction of $\eta/\eta_0$, which is again the manifestation of the saturation effect discussed above. The saturation is more evident in Figure 4b, where we plot $\eta/\eta_0$ directly as a function of $E_0$ for $\mathcal{P} = 0.95\mathcal{P}_{th}$. We observe that, while, for $\omega = \omega_l$, $\eta/\eta_0$ starts to decrease at $E_0 \sim 10^1$ V/m, this happens at larger values of $E_0$ for the other frequencies under consideration. In these cases, the use of the available gain is less efficient, and therefore it is necessary to reach larger values of $E_0$ to substantially saturate the population inversion.

Another important property of localized plasmons is that they produce remarkable extinction cross-sections, usually larger than the geometrical cross-section of the metallic nanostructure that supports them.[2] Figure 4c analyzes the evolution of $\sigma_{ext}/\sigma_{ext,0}$ with $\mathcal{P}$. The results follow the same trends discussed above for $\eta/\eta_0$. Specifically, the largest values of $\sigma_{ext}/\sigma_{ext,0}$ occur for the smallest $E_0$ under consideration at $\omega_l$, reaching a value of ∼20 for $\mathcal{P} = 0.95\mathcal{P}_{th}$. Interestingly, at $\omega_g$ and $\omega_m/\sqrt{3}$, the normalized extinction cross-section first grows and then decreases below one when the pump rate approaches $\mathcal{P} = 0.95\mathcal{P}_{th}$. This means that in these cases the active plasmonic nanoparticle extinguishes less than the passive system. We attribute this behavior to the narrowing of the spectral response of the active plasmonic nanoparticle caused by the increase in the level of gain, which counteracts the global enhancement of the response. As we did for $\eta/\eta_0$, in Figure 4d, we analyze explicitly the dependence of $\sigma_{ext}/\sigma_{ext,0}$ with $E_0$ for $\mathcal{P} = 0.95\mathcal{P}_{th}$. At $\omega_l$, the results show again the effect of saturation. In particular, $\sigma_{ext}/\sigma_{ext,0}$ starts to decrease when $E_0$ reaches $\sim 10^1$ V/m and saturates to one for $E_0 \sim 10^4$ V/m. In contrast, at $\omega_g$ and $\omega_m/\sqrt{3}$, the normalized cross-section displays a nonmonotonic dependence on $E_0$. This behavior is, again, a consequence of the interplay between the narrowing and the global enhancement of the response of the active plasmonic nanoparticle produced by the gain.

## CONCLUSIONS

In summary, we have developed an intuitive yet accurate semianalytical model based on the combination of the semiclassical laser equations for the population dynamics of a 4-level system with the electrostatic solution of the electromagnetic field of a nanosphere. Using this model, we have systematically studied the optical response of a small active plasmonic nanoparticle as a function of both the pump and probe fields. Despite its simplifying assumptions, this model captures the intrinsic nonlinearities associated with the gain for any strength of the probe field and any pump rate below the laser threshold. We have shown that for weak probe fields the response of the active plasmonic nanoparticle, characterized through its polarizability, is greatly enhanced as the pump rate approaches the laser threshold. In particular, the linewidth of the plasmon resonance is remarkably reduced, its peak value is greatly enhanced, and its resonant frequency shifts toward the laser frequency $\omega_l$. All of these effects are the direct consequence of the reduction in the nonradiative losses caused by the presence of gain. This naturally leads to the enhancement of the near- and far-field optical responses of the nanoparticle, which we have illustrated by analyzing the near-field intensity enhancement $\eta$ and the extinction cross-section $\sigma_{ext}$.

In contrast, our model shows as well that the increase in the strength of the probe field leads to a saturation behavior that eventually cancels the effect of the gain. This saturation behavior is caused by the associated increase in the polarization of the free electrons and the gain medium, which depletes the population inversion at a higher rate, thus reducing the gain. In other words, as the probe field strength is increased, the active nanoparticle becomes gradually passive, irrespective of the pump rate. This behavior highlights the necessity of taking into account saturation effects when studying loss-compensated or gain-assisted plasmonic systems, both from theoretical and practical points of view. Importantly, the range of probe field strengths, in which our active nanoparticle transits toward the saturation regime, is of the same order of magnitude as those used experimentally to probe the optical response of loss-compensated plasmonic systems.[9,73] Therefore, when using simplified models to describe the effect of gain, it is important to carefully verify the validity of the approximations because their predictions could lead to an overestimation of the effect of gain. In that sense, our results help to establish the limits of applicability of these models and provide guidelines to improve them.

Since the main goal of adding optical gain to a plasmonic nanostructure is arguably to mitigate its losses and thus improve its optical response, saturation might be seen as an unwanted effect to be avoided. However, it also provides a mechanism to achieve nonlinear behaviors as well as new opportunities for the development of all-optically controlled active nanophotonic devices. As shown in Figure 4, the near-field intensity enhancement as well as the extinction cross-section shows a gradual change of more than 1 order of magnitude with the probe field. Therefore, the nanoparticle behaves effectively as a system that can be reversibly and controllably switched between "on" and "off" states. This effect, which is expected to happen in more complex active plasmonic nanostructures, can be exploited, for instance, to develop actively modulated parity-time symmetric waveguide couplers,[74] metasurfaces,[24] and plasmonic lattices,[40] or as sigmoid-like nonlinear activation functions in parity-time-symmetric optical neural networks.[75] Our results shed light on the behavior of active plasmonic nanostructures and provide the basic understanding needed to exploit these systems to explore novel phenomena such as parity-time symmetry and nonreciprocity.

## ASSOCIATED CONTENT

### Supporting Information

The Supporting Information is available free of charge at https://pubs.acs.org/doi/10.1021/acs.jpcc.2c07558.

Further details of different aspects of the theoretical model (PDF)

## AUTHOR INFORMATION

### Corresponding Author

**Alejandro Manjavacas** − *Instituto de Óptica (IO-CSIC), Consejo Superior de Investigaciones Científicas, 28006 Madrid, Spain; Department of Physics and Astronomy, University of New Mexico, Albuquerque, New Mexico 87106, United States;* orcid.org/0000-0002-2379-1242; Email: a.manjavacas@csic.es



https://doi.org/10.1021/acs.jpcc.2c07558
J. Phys. Chem. C 2023, 127, 2371−2378

## Author

**Luis Cerdán** − *Instituto de Óptica (IO-CSIC), Consejo Superior de Investigaciones Científicas, 28006 Madrid, Spain;* orcid.org/0000-0002-7174-2453

Complete contact information is available at: https://pubs.acs.org/10.1021/acs.jpcc.2c07558


## Notes

The authors declare no competing financial interest.

## ■ ACKNOWLEDGMENTS

This work was sponsored by Grant PID2019-109502GA-I00 funded by MCIN/AEI/10.13039/501100011033 as well as the U.S. National Science Foundation (Grant DMR-1941680). The authors also acknowledge support from a Leonardo Grant for Researchers in Physics from the BBVA Foundation. L.C. also acknowledges partial support from Grant PID2020-114755GB-C31 funded by MCIN/AEI/10.13039/501100011033.

## ■ REFERENCES


(1) Maier, S. A. *Plasmonics: Fundamentals and Applications*; Springer: New York, 2007.

(2) Myroshnychenko, V.; Rodríguez-Fernández, J.; Pastoriza-Santos, I.; Funston, A. M.; Novo, C.; Mulvaney, P.; Liz-Marzán, L. M.; García de Abajo, F. J. Modelling the optical response of gold nanoparticles. *Chem. Soc. Rev.* **2008**, *37*, 1792−1805.

(3) Álvarez-Puebla, R. A.; Liz-Marzán, L. M.; García de Abajo, F. J. Light concentration at the nanometer scale. *J. Phys. Chem. Lett.* **2010**, *1*, 2428−2434.

(4) Baffou, G.; Quidant, R. Nanoplasmonics for chemistry. *Chem. Soc. Rev.* **2014**, *43*, 3898−3907.

(5) Atwater, H. A.; Polman, A. Plasmonics for improved photovoltaic devices. *Nat. Mater.* **2010**, *9*, 205−213.

(6) Anker, J. N.; Hall, W. P.; Lyandres, O.; Shah, N. C.; Zhao, J.; Van Duyne, R. P. Biosensing with plasmonic nanosensors. *Nat. Mater.* **2008**, *7*, 442−453.

(7) Rastinehad, A. R.; Anastos, H.; Wajswol, E.; Winoker, J. S.; Sfakianos, J. P.; Doppalapudi, S. K.; Carrick, M. R.; Knauer, C. J.; Taouli, B.; Lewis, S. C.; et al. Gold nanoshell-localized photothermal ablation of prostate tumors in a clinical pilot device study. *Proc. Natl. Acad. Sci. U. S. A.* **2019**, *116*, 18590−18596.

(8) Khurgin, J. B. How to deal with the loss in plasmonics and metamaterials. *Nat. Nano.* **2015**, *10*, 2−6.

(9) Noginov, M. A.; Podolskiy, V. A.; Zhu, G.; Mayy, M.; Bahoura, M.; Adegoke, J. A.; Ritzo, B. A.; Reynolds, K. Compensation of loss in propagating surface plasmon polariton by gain in adjacent dielectric medium. *Opt. Express* **2008**, *16*, 1385−1392.

(10) Campione, S.; Albani, M.; Capolino, F. Complex modes and near-zero permittivity in 3D arrays of plasmonic nanoshells: loss compensation using gain. *Opt. Mater. Express* **2011**, *1*, 1077−1089.

(11) Xian, J.; Chen, L.; Niu, H.; Qu, J.; Song, J. Significant field enhancements in an individual silver nanoparticle near a substrate covered with a thin gain film. *Nanoscale* **2014**, *6*, 13994−14001.

(12) Song, J.; Xian, J.; Yu, M.; Wang, D.; Ye, S.; Niu, H.; Peng, X.; Qu, J. Ultrahigh enhancement factor by using a silver nanoshell with a gain core above a silver substrate for surface-enhanced Raman scattering at the single-molecule level. *IEEE Photon. J.* **2015**, *7*, 1−8.

(13) Nezhad, M. P.; Tetz, K.; Fainman, Y. Gain assisted propagation of surface plasmon polaritons on planar metallic waveguides. *Opt. Express* **2004**, *12*, 4072−4079.

(14) Noginov, M. A.; Zhu, G.; Bahoura, M.; Adegoke, J.; Small, C. E.; Ritzo, B. A.; Drachev, V. P.; Shalaev, V. M. Enhancement of surface plasmons in an Ag aggregate by optical gain in a dielectric medium. *Opt. Lett.* **2006**, *31*, 3022−3024.

(15) Gather, M. C.; Meerholz, K.; Danz, N.; Leosson, K. Net optical gain in a plasmonic waveguide embedded in a fluorescent polymer. *Nat. Photonics* **2010**, *4*, 457−461.

(16) Li, Z.-Y.; Xia, Y. Metal nanoparticles with gain toward single-molecule detection by surface-enhanced raman scattering. *Nano Lett.* **2010**, *10*, 243−249.

(17) De Leon, I.; Berini, P. Amplification of long-range surface plasmons by a dipolar gain medium. *Nat. Photonics* **2010**, *4*, 382−387.

(18) De Luca, A.; Grzelczak, M. P.; Pastoriza-Santos, I.; Liz-Marzán, L. M.; La Deda, M.; Striccoli, M.; Strangi, G. Dispersed and encapsulated gain medium in plasmonic nanoparticles: a multi-pronged approach to mitigate optical losses. *ACS Nano* **2011**, *5*, 5823−5829.

(19) Hess, O.; Pendry, J. B.; Maier, S. A.; Oulton, R. F.; Hamm, J. M.; Tsakmakidis, K. L. Active nanoplasmonic metamaterials. *Nat. Mater.* **2012**, *11*, 573−584.

(20) Noginov, M. A.; Zhu, G.; Bahoura, M.; Adegoke, J.; Small, C.; Ritzo, B. A.; Drachev, V. P.; Shalaev, V. M. The effect of gain and absorption on surface plasmons in metal nanoparticles. *Appl. Phys. B* **2007**, *86*, 455−460.

(21) Fan, X.; Shen, Z.; Luk'yanchuk, B. Huge light scattering from active anisotropic spherical particles. *Opt. Express* **2010**, *18*, 24868−24880.

(22) Caligiuri, V.; Pezzi, L.; Veltri, A.; De Luca, A. Resonant gain singularities in 1D and 3D metal/dielectric multilayered nanostructures. *ACS Nano* **2017**, *11*, 1012−1025.

(23) Lozano, G.; Louwers, D. J.; Rodríguez, S. R. K.; Murai, S.; Jansen, O. T. A.; Verschuuren, M. A.; Gómez Rivas, J. Plasmonics for solid-state lighting: enhanced excitation and directional emission of highly efficient light sources. *Light Sci. Appl.* **2013**, *2*, No. e241.

(24) Vaskin, A.; Kolkowski, R.; Koenderink, F. A.; Staude, I. Light-emitting metasurfaces. *Nanophotonics* **2019**, *8*, 1151.

(25) Sorger, V. J.; Zhang, X. Spotlight on plasmon lasers. *Science* **2011**, *333*, 709−710.

(26) Berini, P.; De Leon, I. Surface plasmon-polariton amplifiers and lasers. *Nat. Photonics* **2012**, *6*, 16−24.

(27) Yang, A.; Wang, D.; Wang, W.; Odom, T. W. Coherent light sources at the nanoscale. *Annu. Rev. Phys. Chem.* **2017**, *68*, 83−99.

(28) Ma, R.-M.; Oulton, R. F. Applications of nanolasers. *Nat. Nanotechnol.* **2019**, *14*, 12−22.

(29) Bergman, D. J.; Stockman, M. I. Surface plasmon amplification by stimulated emission of radiation: quantum generation of coherent surface plasmons in nanosystems. *Phys. Rev. Lett.* **2003**, *90*, 027402.

(30) Stockman, M. I. Spasers explained. *Nat. Photonics* **2008**, *2*, 327−329.

(31) Noginov, M. A.; Zhu, G.; Belgrave, A. M.; Bakker, R.; Shalaev, V. M.; Narimanov, E. E.; Stout, S.; Herz, E.; Suteewong, T.; Wiesner, U. Demonstration of a spaser-based nanolaser. *Nature* **2009**, *460*, 1110−1112.

(32) Shahbazyan, T. V. Mode volume, energy transfer, and spaser threshold in plasmonic systems with gain. *ACS Photonics* **2017**, *4*, 1003−1008.

(33) Azzam, S. I.; Kildishev, A. V.; Ma, R.-M.; Ning, C.-Z.; Oulton, R.; Shalaev, V. M.; Stockman, M. I.; Xu, J.-L.; Zhang, X. Ten years of spasers and plasmonic nanolasers. *Light Sci. Appl.* **2020**, *9*, 90.

(34) Krasnok, A.; Alú, A. Active nanophotonics. *Proc. IEEE* **2020**, *108*, 628−654.

(35) Benisty, H.; Degiron, A.; Lupu, A.; De Lustrac, A.; Chenais, S.; Forget, S.; Besbes, M.; Barbillon, G.; Bruyant, A.; Blaize, S.; Lérondel, G. Implementation of PT symmetric devices using plasmonics: principle and applications. *Opt. Express* **2011**, *19*, 18004−18019.

(36) Barton, D.; Lawrence, M.; Alaeian, H.; Baum, B.; Dionne, J. *Parity-time Symmetry and Its Applications*; Springer Singapore: Singapore, 2018; Chapter Parity-Time Symmetric Plasmonics, pp 301−349.

(37) Miri, M.-A.; Duggan, R. S.; Alù, A. *Parity-time Symmetry and Its Applications*; Springer Singapore: Singapore, 2018; Chapter Parity-Time Symmetry in Scattering Problems, pp 53−74.

(38) Jin, W.; Khandekar, C.; Pick, A.; Polimeridis, A. G.; Rodriguez, A. W. Amplified and directional spontaneous emission from arbitrary composite bodies: A self-consistent treatment of Purcell effect below threshold. *Phys. Rev. B* **2016**, *93*, 125415.
(39) Zhang, W.; Wu, T.; Zhang, X. Tailoring eigenmodes at spectral singularities in graphene-based PT systems. *Sci. Rep.* **2017**, *7*, 11407.
(40) Kolkowski, R.; Koenderink, A. F. Lattice resonances in optical metasurfaces with gain and loss. *Proc. IEEE* **2020**, *108*, 795−818.
(41) Sanders, S.; Manjavacas, A. Nanoantennas with balanced gain and loss. *Nanophotonics* **2020**, *9*, 473−480.
(42) Manjavacas, A. Anisotropic optical response of nanostructures with balanced gain and loss. *ACS Photonics* **2016**, *3*, 1301−1307.
(43) Miri, M.-A.; Eftekhar, M. A.; Facao, M.; Abouraddy, A. F.; Bakry, A.; Razvi, M. A. N.; Alshahrie, A.; Alú, A.; Christodoulides, D. N. Scattering properties of PT-symmetric objects. *J. Opt.* **2016**, *18*, 075104.
(44) Duggan, R.; Miri, M.-A.; Alù, A. Scattering properties of parity-time symmetric nanoparticle dimers. *2017 IEEE International Symposium on Antennas and Propagation*; USNC/URSI National Radio Science Meeting. 2017; pp 1067−1068.
(45) Safari, M.; Albooyeh, M.; Simovski, C. R.; Tretyakov, S. A. Shadow-free multimers as extreme-performance meta-atoms. *Phys. Rev. B* **2018**, *97*, 085412.
(46) Krasnok, A.; Baranov, D.; Li, H.; Miri, M.-A.; Monticone, F.; Alú, A. Anomalies in light scattering. *Adv. Opt. Photon.* **2019**, *11*, 892−951.
(47) Kolkowski, R.; Koenderink, A. F. Gain-induced scattering anomalies of diffractive metasurfaces. *Nanophotonics* **2020**, *9*, 4273.
(48) Zhang, Y. J.; Li, P.; Galdi, V.; Tong, M. S.; Alù, A. Manipulating the scattering pattern with non-Hermitian particle arrays. *Opt. Express* **2020**, *28*, 19492−19507.
(49) Tapar, J.; Kishen, S.; Emani, N. K. Dynamically tunable asymmetric transmission in PT-symmetric phase gradient metasurface. *ACS Photonics* **2021**, *8*, 3315−3322.
(50) Liang, Y.; Gaimard, Q.; Klimov, V.; Uskov, A.; Benisty, H.; Ramdane, A.; Lupu, A. Coupling of nanoantennas in loss-gain environment for application in active tunable metasurfaces. *Phys. Rev. B* **2021**, *103*, 045419.
(51) Türeci, H. E.; Stone, A. D.; Collier, B. Self-consistent multimode lasing theory for complex or random lasing media. *Phys. Rev. A* **2006**, *74*, 043822.
(52) Fang, A.; Koschny, T.; Wegener, M.; Soukoulis, C. M. Self-consistent calculation of metamaterials with gain. *Phys. Rev. B* **2009**, *79*, 241104.
(53) Andresen, M. P. H.; Skaldebø, A. V.; Haakestad, M. W.; Krogstad, H. E.; Skaar, J. Effect of gain saturation in a gain compensated perfect lens. *J. Opt. Soc. Am. B* **2010**, *27*, 1610−1616.
(54) Baranov, D. G.; Andrianov, E.; Vinogradov, A. P.; Lisyansky, A. A. Exactly solvable toy model for surface plasmon amplification by stimulated emission of radiation. *Opt. Express* **2013**, *21*, 10779−10791.
(55) Arnold, N.; Piglmayer, K.; Kildishev, A. V.; Klar, T. A. Spasers with retardation and gain saturation: electrodynamic description of fields and optical cross-sections. *Opt. Mater. Express* **2015**, *5*, 2546−2577.
(56) Barton, D. R.; Alaeian, H.; Lawrence, M.; Dionne, J. Broadband and wide-angle nonreciprocity with a non-Hermitian metamaterial. *Phys. Rev. B* **2018**, *97*, 045432.
(57) Fietz, C.; Soukoulis, C. M. Finite element simulation of microphotonic lasing system. *Opt. Express* **2012**, *20*, 11548−11560.
(58) Cuerda, J.; García-Vidal, F. J.; Bravo-Abad, J. Spatio-temporal modeling of lasing action in core-shell metallic nanoparticles. *ACS Photonics* **2016**, *3*, 1952−1960.
(59) Siegman, A. *Lasers*; University Science Books: 1986.
(60) Cerjan, A.; Chong, Y.; Ge, L.; Stone, A. D. Steady-state ab initio laser theory for N-level lasers. *Opt. Express* **2012**, *20*, 474−488.
(61) Jackson, J. D. *Classical Electrodynamics*; Wiley: New York, 1975.
(62) Ma, R.-M.; Ota, S.; Li, Y.; Yang, S.; Zhang, X. Explosives detection in a lasing plasmon nanocavity. *Nat. Nanotechnol.* **2014**, *9*, 600−604.
(63) Wang, X.-Y.; Wang, Y.-L.; Wang, S.; Li, B.; Zhang, X.-W.; Dai, L.; Ma, R.-M. Lasing enhanced surface plasmon resonance sensing. *Nanophotonics* **2017**, *6*, 472−478.
(64) Meng, L.; Zhao, D.; Yang, Y.; García de Abajo, F. J.; Li, Q.; Ruan, Z.; Qiu, M. Gain-assisted plasmon resonance narrowing and its application in sensing. *Phys. Rev. Appl.* **2019**, *11*, 044030.
(65) Kim, J.; Naik, G. V.; Emani, N. K.; Guler, U.; Boltasseva, A. Plasmonic resonances in nanostructured transparent conducting oxide films. *IEEE J. Sel. Topics Quantum Electron.* **2013**, *19*, 4601907−4601907.
(66) Agrawal, A.; Cho, S. H.; Zandi, O.; Ghosh, S.; Johns, R. W.; Milliron, D. J. Localized surface plasmon resonance in semiconductor nanocrystals. *Chem. Rev.* **2018**, *118*, 3121−3207.
(67) Xu, H.; Suslick, K. S. Water-soluble fluorescent silver nanoclusters. *Adv. Mater.* **2010**, *22*, 1078−1082.
(68) Zheng, J.; Zhou, C.; Yu, M.; Liu, J. Different sized luminescent gold nanoparticles. *Nanoscale* **2012**, *4*, 4073−4083.
(69) Chen, W.; Roelli, P.; Ahmed, A.; Verlekar, S.; Hu, H.; Banjac, K.; Lingenfelder, M.; Kippenberg, T. J.; Tagliabue, G.; Galland, C. Intrinsic luminescence blinking from plasmonic nanojunctions. *Nat. Commun.* **2021**, *12*, 2731.
(70) Khandekar, C.; Jin, W.; Miller, O. D.; Pick, A.; Rodriguez, A. W. Giant frequency-selective near-field energy transfer in active-passive structures. *Phys. Rev. B* **2016**, *94*, 115402.
(71) Cerdán, L. Ultrashort pulse generation in nanolasers by means of Lorenz-Haken instabilities. *Ann. Phys. (Berlin, Ger.)* **2021**, *533*, 2100122.
(72) Zundel, L.; Gieri, P.; Sanders, S.; Manjavacas, A. Comparative analysis of the near- and far-field optical response of thin plasmonic nanostructures. *Adv. Opt. Mater.* **2022**, *10*, 2102550.
(73) Seidel, J.; Grafström, S.; Eng, L. Stimulated emission of surface plasmons at the interface between a silver film and an optically pumped dye solution. *Phys. Rev. Lett.* **2005**, *94*, 177401.
(74) Lupu, A.; Benisty, H.; Degiron, A. Switching using PT symmetry in plasmonic systems: positive role of the losses. *Opt. Express* **2013**, *21*, 21651−21668.
(75) Deng, H.; Khajavikhan, M. Parity−time symmetric optical neural networks. *Optica* **2021**, *8*, 1328−1333.


https://doi.org/10.1021/acs.jpcc.2c07558
J. Phys. Chem. C 2023, 127, 2371−2378

# Supporting Information: Analysis of the Limits of the Optical Response of a Metallic Nanoparticle with Gain

Luis Cerdán[†] and Alejandro Manjavacas[*,†,‡]

†*Instituto de Óptica (IO-CSIC), Consejo Superior de Investigaciones Científicas, 28006 Madrid, Spain*

‡*Department of Physics and Astronomy, University of New Mexico, Albuquerque, New Mexico 87106, United States*

E-mail: a.manjavacas@csic.es

## Solution of Maxwell's equations for a small nanoparticle

We consider a spherical nanoparticle with a radius $R$ excited by an electric field $\mathbf{E}_0$. Assuming that the size of the nanoparticle is much smaller than the wavelength of the electric field, we can exploit the electrostatic approximation to calculate the total field inside the nanoparticle[S1] (in Gaussian units) as

$$\mathbf{E}_\mathrm{t} = -\frac{4\pi}{3}\mathbf{P} + \mathbf{E}_0.$$

Here, $\mathbf{P}$ represents the total polarization of the nanoparticle, which, in this limit, is uniform. In our particular case, $\mathbf{P}$ corresponds to the sum of the polarization due to the free electrons $\mathbf{P}_\mathrm{m}$ and the polarization of the gain medium $\mathbf{P}_\mathrm{g}$. Notice that this expression does not depend on the frequency of the external field and therefore applies to both frequency and time domains.[S2] Within the same limit, the total field at a point $\mathbf{r} = r\hat{\mathbf{r}}$ outside of the nanoparticle is given by

$$\mathbf{E}_\mathrm{t} = \mathbf{E}_0 + \frac{1}{r^3}\left[3\hat{\mathbf{r}}(\hat{\mathbf{r}}\cdot\mathbf{p}) - \mathbf{p}\right],$$

where $\mathbf{p} = V\left(\mathbf{P}_\mathrm{m} + \mathbf{P}_\mathrm{g}\right)$ is the total dipole moment of the nanoparticle.

## Time-domain equations for the response of the active plasmonic nanoparticle

Starting from Equations (1)-(3) of the main text, assuming that all of the vectors are parallel to $\mathbf{E}_0$, and using the decomposition $F(t) = fe^{-i\omega t} + f^* e^{i\omega t}$, with $f$ being a slowly varying complex magnitude, we obtain

$$\ddot{P}_\mathrm{m} + \dot{P}_\mathrm{m}\left(-2i\omega + 2\Gamma_\mathrm{m}\right) + P_\mathrm{m}\left(\frac{\omega_\mathrm{m}^2}{3} - \omega^2 - 2i\Gamma_\mathrm{m}\omega\right) = -\frac{\omega_\mathrm{m}^2}{3}P_\mathrm{g} + \frac{\omega_\mathrm{m}^2}{4\pi}E_0, \tag{S1}$$

$$\ddot{P}_\mathrm{g} + \dot{P}_\mathrm{g}\left(-2i\omega + 2\Gamma_\mathrm{g}\right) + P_\mathrm{g}\left(\omega_\mathrm{g}^2 - \omega^2 - 2i\Gamma_\mathrm{g}\omega - \frac{4\pi}{3}\sigma_\mathrm{g}\Delta N\right) = \sigma_\mathrm{g}\Delta N\left(\frac{4\pi}{3}P_\mathrm{m} - E_0\right), \tag{S2}$$

where we use dots to denote time derivatives. Similarly, the equations describing the dynamics of the population densities of the different levels read

$$\begin{aligned}
\dot{N}_3 &= -\gamma_{32}N_3 + \mathcal{P}(N_0 - N_3),\\
\dot{N}_2 &= \gamma_{32}N_3 - \gamma_{21}N_2 + \frac{2}{\hbar\omega_{\rm g}}\mathrm{Re}\left\{\left(E_0 - \frac{4\pi}{3}P_{\rm m}\right)\left(i\omega P_{\rm g}^* + \dot{P}_{\rm g}^*\right) - \frac{4\pi}{3}P_{\rm g}\dot{P}_{\rm g}^*\right\},\\
\dot{N}_1 &= \gamma_{21}N_2 - \gamma_{10}N_1 - \frac{2}{\hbar\omega_{\rm g}}\mathrm{Re}\left\{\left(E_0 - \frac{4\pi}{3}P_{\rm m}\right)\left(i\omega P_{\rm g}^* + \dot{P}_{\rm g}^*\right) - \frac{4\pi}{3}P_{\rm g}\dot{P}_{\rm g}^*\right\},\\
\dot{N}_0 &= \gamma_{10}N_1 - \mathcal{P}(N_0 - N_3),
\end{aligned} \tag{S3}$$

where the terms that depend on the probe field and polarizations have been averaged over a period.

## Steady-state solution

Equations (5)-(7) of the main text correspond to the steady-state (SS) solution for Equations (S1)-(S3), and form a system of coupled nonlinear equations that does not have a general analytical solution. The key to making the solution more tractable from a computational point of view is to explicitly decompose the polarizations into their real and imaginary parts. By doing so, Equations (5) and (6) of the main text become

$$\begin{aligned}
P_{\rm m}^{\rm SS,r} &= -\frac{\omega_{\rm m}^2/3}{\mu_1^2+\mu_2^2}\left[\left(P_{\rm g}^{\rm SS,r} - \frac{3}{4\pi}E_0\right)\mu_1 - P_{\rm g}^{\rm SS,i}\mu_2\right],\\
P_{\rm m}^{\rm SS,i} &= -\frac{\omega_{\rm m}^2/3}{\mu_1^2+\mu_2^2}\left[\left(P_{\rm g}^{\rm SS,r} - \frac{3}{4\pi}E_0\right)\mu_2 + P_{\rm g}^{\rm SS,i}\mu_1\right],
\end{aligned} \tag{S4}$$

$$\begin{aligned}
P_{\rm g}^{\rm SS,r} &= \frac{\sigma_{\rm g}\Delta N^{\rm SS}}{\left(\pi_1 - \frac{4\pi}{3}\sigma_{\rm g}\Delta N^{\rm SS}\right)^2 + \pi_2^2}\left[\left(\frac{4\pi}{3}P_{\rm m}^{\rm SS,r} - E_0\right)\left(\pi_1 - \frac{4\pi}{3}\sigma_{\rm g}\Delta N^{\rm SS}\right) - \frac{4\pi}{3}P_{\rm m}^{\rm SS,i}\pi_2\right],\\
P_{\rm g}^{\rm SS,i} &= \frac{\sigma_{\rm g}\Delta N^{\rm SS}}{\left(\pi_1 - \frac{4\pi}{3}\sigma_{\rm g}\Delta N^{\rm SS}\right)^2 + \pi_2^2}\left[\left(\frac{4\pi}{3}P_{\rm m}^{\rm SS,r} - E_0\right)\pi_2 + \frac{4\pi}{3}P_{\rm m}^{\rm SS,i}\left(\pi_1 - \frac{4\pi}{3}\sigma_{\rm g}\Delta N^{\rm SS}\right)\right],
\end{aligned} \tag{S5}$$

while

$$\Delta N^{\rm SS} = \nu_1 + \nu_2\omega\left[E_0 P_{\rm g}^{\rm SS,i} - \frac{4\pi}{3}\left(P_{\rm m}^{\rm SS,r}P_{\rm g}^{\rm SS,i} - P_{\rm m}^{\rm SS,i}P_{\rm g}^{\rm SS,r}\right)\right]. \tag{S6}$$

In these expressions, we have introduced the following definitions:

$$\mu_1 = \omega_{\mathrm{m}}^2/3 - \omega^2,$$

$$\mu_2 = 2\Gamma_{\mathrm{m}}\omega,$$

$$\pi_1 = \omega_{\mathrm{g}}^2 - \omega^2,$$

$$\pi_2 = 2\Gamma_{\mathrm{g}}\omega,$$

$$\nu_1 = \frac{S\mathcal{P}N_{\mathrm{t}}}{\gamma_{10} + \mathcal{P}\left(2 + 2\frac{\gamma_{10}}{\gamma_{32}} + S\right)},$$

$$\nu_2 = \frac{2}{\gamma_{21}\hbar\omega_{\mathrm{g}}}\left[1 - \frac{S\mathcal{P}}{\gamma_{10} + \mathcal{P}\left(2 + 2\frac{\gamma_{10}}{\gamma_{32}} + S\right)}\right].$$

We could subsequently substitute Equations (S4) and (S6) into (S5) to obtain a rather convoluted system of two coupled equations, which would only depend on $P_{\mathrm{g}}^{\mathrm{SS,r}}$ and $P_{\mathrm{g}}^{\mathrm{SS,i}}$. While such an approach is feasible, it is more convenient to directly solve the system of Equations (S4)-(S6) by converting it into a two-dimensional *root-finding* problem where the root is $(P_{\mathrm{g}}^{\mathrm{SS,r}}, P_{\mathrm{g}}^{\mathrm{SS,i}})$. Once $P_{\mathrm{g}}^{\mathrm{SS,r}}$ and $P_{\mathrm{g}}^{\mathrm{SS,i}}$ are found, we substitute them into (S4) to obtain $P_{\mathrm{m}}^{\mathrm{SS,r}}$ and $P_{\mathrm{m}}^{\mathrm{SS,i}}$ and, with them, $\Delta N^{\mathrm{SS}}$ using Equation (S6).

## Laser threshold and frequency

The laser threshold and frequency are fundamental properties of any laser system and, as such, have been treated extensively in the literature.[S3–S7] In principle, they can be determined by analyzing the complex poles of the optical response of the system. Here, we instead follow the lead of previous works on dynamical instabilities, and calculate the laser threshold pump rate $\mathcal{P}_{\mathrm{th}}$ and the laser frequency $\omega_{\mathrm{l}}$ of the active nanoparticle by performing a linear stability analysis on the system of equations formed by Equations (S1)-(S3).

In absence of a probe field, there is a trivial steady-state solution for these equations, namely $P_{\mathrm{m}}^{\mathrm{SS}} = P_{\mathrm{g}}^{\mathrm{SS}} = 0$, $\Delta N^{\mathrm{SS}} = \nu_1$ (*cf.* Equations. (5)-(7) in the main text). At threshold, this trivial solution becomes unstable and the system evolves towards a nontrivial steady-

state solution with $P_{\rm m}^{\rm SS} \neq P_{\rm g}^{\rm SS} \neq 0$. To find the conditions for which the trivial solution becomes unstable, we try $P_{\rm m} = \delta P_{\rm m} e^{\Gamma t}$ and $P_{\rm g} = \delta P_{\rm g} e^{\Gamma t}$, where $\delta P_{\rm m}$ and $\delta P_{\rm g}$ are constants representing infinitesimally small perturbations. Substituting these expressions into Equations (S1) and (S2), we have

$$\begin{aligned}
&\left[\Gamma^2 + \Gamma\left(-2i\omega + 2\Gamma_{\rm m}\right) + \left(\frac{\omega_{\rm m}^2}{3} - \omega^2 - 2i\Gamma_{\rm m}\omega\right)\right]\delta P_{\rm m} = -\frac{\omega_{\rm m}^2}{3}\delta P_{\rm g}, \\
&\left[\Gamma^2 + \Gamma\left(-2i\omega + 2\Gamma_{\rm g}\right) + \left(\omega_{\rm g}^2 - \omega^2 - 2i\Gamma_{\rm g}\omega - \frac{4\pi}{3}\sigma_{\rm g}\nu_1\right)\right]\delta P_{\rm g} = \frac{4\pi}{3}\sigma_{\rm g}\nu_1\delta P_{\rm m}.
\end{aligned} \tag{S7}$$

When the system is at threshold, the perturbations must neither increase nor decrease, so, accordingly, $\Gamma = 0$. Then, the equations above reduce to the following linear system:

$$A\begin{pmatrix}\delta P_{\rm m} \\ \delta P_{\rm g}\end{pmatrix} = \begin{pmatrix}0 \\ 0\end{pmatrix},$$

with the matrix $A$ being

$$A = \begin{pmatrix}\omega_{\rm m}^2/3 - \omega^2 - 2i\Gamma_{\rm m}\omega & \omega_{\rm m}^2/3 \\ -\frac{4\pi}{3}\sigma_{\rm g}\nu_1 & \omega_{\rm g}^2 - \omega^2 - 2i\Gamma_{\rm g}\omega - \frac{4\pi}{3}\sigma_{\rm g}\nu_1\end{pmatrix}.$$

Then, to find the laser threshold pump rate $\mathcal{P}_{\rm th}$ and frequency $\omega_{\rm l}$, we search for the values of $\nu_1$ and $\omega$ that make the real and imaginary parts of $\det\{A\}$ simultaneously zero. To that end, we employ, again, a two-dimensional *root-finding* algorithm. Once we know these solutions, we calculate $\mathcal{P}_{\rm th}$ as

$$\mathcal{P}_{\rm th} = \frac{\nu_1\gamma_{10}}{SN_t - \nu_1\left(2 + 2\gamma_{10}/\gamma_{32} + S\right)}.$$

# References


[S1] Jackson, J. D. *Classical Electrodynamics*; Wiley: New York, 1975.

[S2] Jefimenko, O. D. Solutions of Maxwell's equations for electric and magnetic fields in arbitrary media. *Am. J. Phys.* **1992**, *60*, 899–902.

[S3] Shahbazyan, T. V. Mode volume, energy transfer, and spaser threshold in plasmonic systems with gain. *ACS Photonics* **2017**, *4*, 1003–1008.

[S4] Vyshnevyy, A. A.; Fedyanin, D. Y. Lasing threshold of thresholdless and non-thresholdless metal-semiconductor nanolasers. *Opt. Express* **2018**, *26*, 33473–33483.

[S5] Ma, R.-M.; Oulton, R. F. Applications of nanolasers. *Nat. Nanotechnol.* **2019**, *14*, 12–22.

[S6] Azzam, S. I.; Kildishev, A. V.; Ma, R.-M.; Ning, C.-Z.; Oulton, R.; Shalaev, V. M.; Stockman, M. I.; Xu, J.-L.; Zhang, X. Ten years of spasers and plasmonic nanolasers. *Light Sci. Appl.* **2020**, *9*, 90.

[S7] Cerdán, L. Ultrashort pulse generation in nanolasers by means of Lorenz-Haken instabilities. *Ann. Phys. (Berlin, Ger.)* **2021**, *533*, 2100122.